# Free-energy-based reduced transport model for bistability and hysteresis in plasma turbulence

T. Izuka[1], E. Narita[1, 2], S. Maeyama[2]

[1]*Kyoto University, Kyoto, Kyoto 615-8540, Japan*

[2]*National Institute for Fusion Science, Toki, Gifu 509-5292, Japan*

## Introduction

Transport bifurcation and hysteresis are important challenges in reduced modeling of plasma turbulence. Conventional transport models generally assume that the turbulent heat flux is uniquely determined by plasma parameters such as the temperature gradient and the background $E \times B$ flow shear. Near a critical regime, however, nonlinear turbulence simulations show that low- and high-transport states can coexist under the same equilibrium conditions [1, 2]. The final saturated state can depend on the initial perturbation amplitude and the initial fluctuation pattern.

This bistability implies that a single-valued closure may be insufficient because the same plasma parameters can correspond to different turbulent heat fluxes. An additional variable describing the turbulent state is therefore required. In this work, we first demonstrate probabilistic state selection in the bistable regime using local gyrokinetic simulations. We then characterize the wave-number-space dynamics and identify its poloidal lap average as a slowly varying state variable. Based on this variable, we construct a phenomenological double-well pseudo-free-energy model for stochastic state selection and discuss its extension to a history-dependent transport closure.

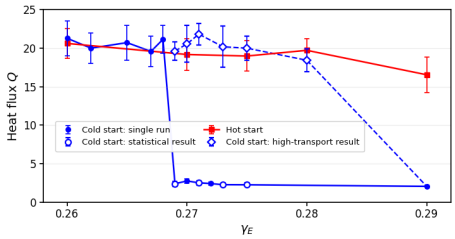


Figure 1: Comparison of the heat flux for different initial perturbation amplitudes. Simulation results for cold start (blue) and hot start (red).

## Bistability in gyrokinetic simulations

Local gyrokinetic simulations were performed for several values of the equilibrium flow shear, $\gamma_E$, using the rotating-flux-tube implementation of the GKV code [3, 4]. Here, two initial fluctuation amplitudes were considered. Small and large initial fluctuation amplitudes are referred to as cold and hot starts, respectively. As shown in Figure 1, at relatively weak shear, both initial conditions approach a high-transport turbulent state. At sufficiently strong shear, the fluctuations are suppressed and the system approaches a low-transport state. Between these regimes, a bistable region appears in which the hot-start simulations generally maintain

| $\gamma_E$ | High-transport cases | Observed fraction |
|---|---|---|
| 0.267 | 12/20 | 0.60 |
| 0.269 | 10/20 | 0.50 |
| 0.271 | 8/20 | 0.40 |
| 0.273 | 6/20 | 0.30 |
| 0.275 | 5/20 | 0.25 |

Table 1: Number of cold-start simulations reaching the high-transport state. Twenty different random seeds were used for each value of $\gamma_E$.

a large heat flux, whereas the cold-start simulations can approach either transport state.

Table 1 shows the number of cold-start simulations that eventually reached the high-transport state.

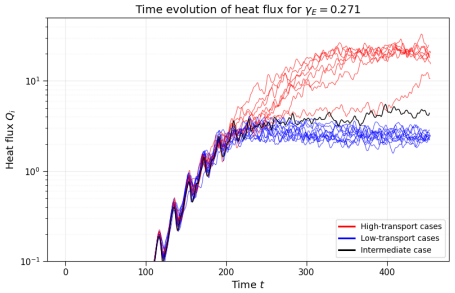


Figure 2: Time evolution of the ion heat flux for $\gamma_E = 0.271$. Red, blue, and black curves represent high-transport, low-transport, and a long-lived intermediate case, respectively.

Although the equilibrium conditions and the initial fluctuation amplitude are identical for simulations at the same $\gamma_E$, different random seeds used to generate the initial fluctuation pattern can lead to different final transport states. As an example, Fig. 2 shows the time evolution of the heat flux for 20 cold-start simulations at $\gamma_E = 0.271$, each initialized with a different random seed. This result demonstrates that the transition is not described by a unique deterministic threshold. Instead, the final saturated state is selected probabilistically through the competition between shear-induced suppression and nonlinear turbulent growth. In this sense, even at a fixed value of $\gamma_E$, both transport states remain accessible, showing that fluctuation history and nonlinear mode coupling play essential roles in the state selection.

**Wave-number-space characterization**

The equilibrium flow shear continuously deforms the non-zonal fluctuation spectrum in the $(k_x, k_y)$ plane, producing a preferential spectral tilt. To quantify both the direction and magnitude of this tilt, we introduce the signed spectral-tilt measure

$$C_{xy}(t) = \sum_{k_x,k_y>0} k_x k_y \left\langle \left|\phi(k_x,k_y,z;t)\right|^2 \right\rangle_z \Big/ \sum_{k_x,k_y>0} \left\langle \left|\phi(k_x,k_y,z;t)\right|^2 \right\rangle_z . \tag{1}$$

Here, $k_x$ and $k_y$ denote the radial and binormal wave numbers, respectively, $\phi(k_x,k_y,z;t)$ is the electrostatic potential, $z$ is the field-aligned coordinate, and $t$ denotes time. The brackets $\langle\cdot\rangle_z$ represent an average along the field-aligned direction [3]. The simulations show that $C_{xy}$ oscillates approximately with the poloidal-lap (Floquet-mode oscillation) period, $T_{\mathrm{lap}} = 2\pi\hat{s}/|\gamma_E|$, where $\hat{s}$ is the magnetic shear. Although this periodic motion is not clearly visible in the heat flux after the linear growth phase, it remains an essential feature of the wave-number-space dynamics. We

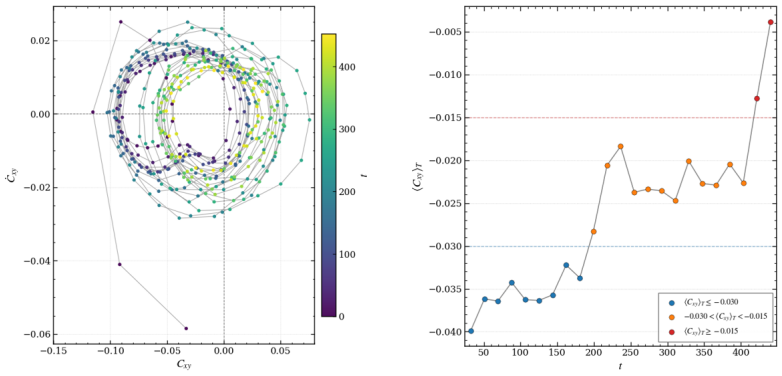

(a) (b)

Figure 3: Representative wave-number-space dynamics in two different simulations. (a) Trajectory in the projected space $(C_{xy}, \dot{C}_{xy})$ for a simulation that reaches the high-transport state. (b) Time evolution of $\overline{C}_{xy}^{(T)}$ for another simulation that remains in an intermediate state before transitioning to the high-transport state.

then define $\overline{C}_{xy}^{(T)}$ as the average of $C_{xy}$ over one poloidal lap period. In the projected state space $(C_{xy}, \dot{C}_{xy})$, where $\dot{C}_{xy} \equiv dC_{xy}/dt$, the oscillatory trajectories form loops whose centers depend on the transport state. In the low-transport state, the trajectories remain biased toward negative $C_{xy}$. By contrast, in the high-transport state (Fig. 3(a)), the center shifts toward $C_{xy} \simeq 0$, and the trajectory generally extends into the positive-$C_{xy}$ region. Thus, for the cold-start simulations, different random initial fluctuation patterns can lead to either transport state even at the same $\gamma_E$, whereas such state selection has not yet been observed for the hot-start simulations.

**Pseudo-free-energy model**

As demonstrated in the previous section, $\overline{C}_{xy}^{(T)}$ clearly distinguishes the low- and high-transport states. To construct a phenomenological double-well potential based on this quantity, we define the dimensionless effective state variable $c = (\overline{C}_{xy}^{(T)} - C_b)/\Delta C, C_b \simeq -0.02$, where $C_b$ is the approximate boundary between the low- and high-transport regions and $\Delta C$ characterizes their separation. With this definition, $c < 0$ and $c > 0$ predominantly correspond to the low- and high-transport states, respectively. We then construct a phenomenological double-well pseudo-free energy from a mixture of distributions associated with the two states:

$$F(c;s) = -\ln\left[s\exp\left\{-(c+1)^2/2\sigma_{\mathrm{L}}^2\right\} + (1-s)\exp\left\{-(c-1)^2/2\sigma_{\mathrm{H}}^2\right\}\right]. \tag{2}$$

Here, $c = -1$ and $c = 1$ represent the low- and high-transport states, respectively. The parameters $\sigma_{\mathrm{L}}$ and $\sigma_{\mathrm{H}}$ characterize the fluctuation widths of the two states.

The parameter $s$ controls the relative statistical preference for the two transport states: larger $s$ favors the low-transport state, whereas smaller $s$ favors the high-transport state. We assume phenomenologically that $s$ depends on an effective shear, $\gamma_{\mathrm{eff}} = |\gamma_E + \gamma_Z(c)|$, where $\gamma_E$ is the equilibrium flow shear and $\gamma_Z$ represents the shear generated by zonal flows. Since stronger effective shear favors turbulence suppression, we assume $\partial s/\partial \gamma_{\mathrm{eff}} > 0$.

The temporal evolution of the effective state variable $c$ is described by a Langevin equation,

$$\frac{dc}{dt} = -\mu \frac{dF}{dc} + \xi(t), \tag{3}$$

where $\mu$ is a response coefficient and $\xi(t)$ represents effective stochastic forcing arising from unresolved turbulent degrees of freedom. The two minima of $F$ correspond to the low- and high-transport quasi-stationary states, while the maximum between them acts as an effective transition barrier.

This framework connects the observed state selection to both the initial perturbation and turbulent fluctuations. For a large initial perturbation, nonlinear interactions overcome the shear-induced spectral bias within the first poloidal lap period, bringing $c$ close to zero and enabling entry into the high-transport basin. For a small initial perturbation, the equilibrium shear suppresses the fluctuations before strong nonlinear interactions develop, and the system is therefore more likely to remain in the low-transport basin. Long-lived intermediate behavior may arise when the zonal-flow contribution causes the effective shear, and hence the potential landscape, to evolve slowly in time. Thus, even for the same cold-start amplitude and the same $\gamma_E$, different random initial fluctuation patterns can lead to either transport state. A slow variation of the equilibrium flow shear $\gamma_E$ changes the relative depths of the two wells and can produce hysteresis through metastable trapping.

## Conclusions

Local gyrokinetic simulations show that low- and high-transport states can coexist under identical equilibrium conditions, with the final state selected probabilistically by the initial perturbation amplitude and random seed. In the high-transport state, nonlinear dynamics compensate for the shear-induced spectral bias, shifting $\overline{C}_{xy}^{(T)}$ toward zero. This motivates its use as an effective state variable in a double-well pseudo-free-energy model of bistability, stochastic state selection, and hysteresis. Future work will clarify the mechanisms underlying subcritical phenomena such as bistability and hysteresis, and develop the present framework into a predictive transport model for plasma temperature evolution.

## References


[1] B. F. McMillan et al., J. Plasma Phys. **84** (2018), 905840611

[2] N. Christen et al., J. Plasma Phys. **88** (2022), 905880504

[3] S. Maeyama et al., J. Comput. Phys. **522** (2025) 113595

[4] T.-H. Watanabe and H. Sugama, Nucl. Fusion **46** (2006) 24-32